Age-related morphological changes of the dermal matrix in human skin documented *in vivo* by multiphoton microscopy

Hequn Wang
Thomas Shyr
Michael J. Fevola
Gabriela Oana Cula
Georgios N. Stamatas

Age-related morphological changes of the dermal matrix in human skin documented *in vivo* by multiphoton microscopy

Hequn Wang,[a] Thomas Shyr,[a] Michael J. Fevola,[a] Gabriela Oana Cula,[a] and Georgios N. Stamatas[b,*]

[a]Johnson & Johnson Consumer Inc., Beauty Innovation Platforms, Skillman, New Jersey, United States
[b]Johnson & Johnson Santé Beauté, Global Consumer R&D, Issy-les-Moulineaux, France

Abstract. Two-photon fluorescence (TPF) and second harmonic generation (SHG) microscopy provide direct visualization of the skin dermal fibers *in vivo*. A typical method for analyzing TPF/SHG images involves averaging the image intensity and therefore disregarding the spatial distribution information. The goal of this study is to develop an algorithm to document age-related effects of the dermal matrix. TPF and SHG images were acquired from the upper inner arm, volar forearm, and cheek of female volunteers of two age groups: 20 to 30 and 60 to 80 years of age. The acquired images were analyzed for parameters relating to collagen and elastin fiber features, such as orientation and density. Both collagen and elastin fibers showed higher anisotropy in fiber orientation for the older group. The greatest difference in elastin fiber anisotropy between the two groups was found for the upper inner arm site. Elastin fiber density increased with age, whereas collagen fiber density decreased with age. The proposed analysis considers the spatial information inherent to the TPF and SHG images and provides additional insights into how the dermal fiber structure is affected by the aging process. © *The Authors. Published by SPIE under a Creative Commons Attribution 3.0 Unported License. Distribution or reproduction of this work in whole or in part requires full attribution of the original publication, including its DOI.* [DOI: 10.1117/1.JBO.23.3.030501]

Certain structural and morphological changes of the skin tissue are associated with the aging process. These changes involve mainly the extracellular matrix components collagen, elastin, proteoglycans, fibronectin, etc.[1] Recently, several optical methods, such as reflectance confocal microscopy[2,3] and optical coherence tomography[4] that provide direct visualization of the inner skin structures noninvasively, have been developed to study the skin aging process. Multiphoton microscopy (MPM) offers direct visualization of collagen and elastin fibers simultaneously, using the two-photon fluorescence (TPF) and second harmonic generation (SHG) imaging channels, respectively.[5] Its unique capability to separate the SHG signals of collagen fibers from elastin autofluorescence (AF) has confirmed MPM as an ideal method to investigate skin aging. For example, by analyzing the mean intensity changes of collagen and elastin fibers, the SHG-to-AF aging index of dermis (SAAID) was defined and found to decrease with age.[6] In addition to intrinsic aging, photoaging has also been studied by comparing the differences in SAAID between sun-exposed and sun-protected skin regions.[7] However, this method ignores the information relating to the spatial distribution of the signals. One method that has been proposed to address this limitation involves the use of the fast Fourier-transform analysis to evaluate the orientation and bundle packing of collagen fibers in mouse skin.[8] In this study, we propose a different approach to analyze the spatial distribution of the SHF and AF signals. We use this approach to characterize the orientation and density of collagen and elastin fibers, which provides insights into the age-related remodeling of the dermal matrix.

The MPM system used in this study was a commercial MPTflex™ system (JenLab GmbH, Jena, Germany), which uses a tunable near-infrared femtosecond laser for excitation. The excitation wavelength was 820 nm, and the irradiation power at the skin surface was <50 mW. TPF and SHG signals were collected at distinct wavelength ranges such as 409 to 680 nm and 373 to 387 nm, respectively. For each subject, three image stacks (from 20 μm above the skin surface to 120-μm beneath the skin surface with a step size of 5 μm) were acquired. The image field was 200 μm × 200 μm corresponding to 512 × 512 pixels. Z-stacks of TPF and SHG images were also taken at three different body sites including the dorsal forearm, upper inner arm, and cheek. Twenty female volunteers equally split between two age groups such as 20 to 30 and 60 to 80 years of age were recruited for this study following a signed informed consent. The study was approved by the Landesärztekammer Thüringen ethics committee (Jena, Germany). Image analysis to characterize the dermal fiber alterations was performed. Due to the field curvature and the uneven topology of the skin layers, the dermal fibers appeared at different frames and areas within each frame. For example, in some images half of the field-of-view was occupied by cellular structures of the epidermis and the other half with dermal fibers. For a standardized analysis, a region of interest (ROI) of 200 × 200 pixels with relatively rich fiber coverage was selected for each frame.

Dermal fibers were easily identified in the TPF and SHG images of the younger skin group, with elastin fibers shown as thin distinct bundles [Fig. 1(a)], whereas collagen fibers shown as thick intertwined bundles [Fig. 1(b)]. In Fig. 1(c), the false-color overlay image, with red representing elastin fibers and green representing collagen fibers, shows that the two types of fibers spatially intertwine with each other, with almost no overlaps. In the aged group, elastin fibers assumed a tortuous and patchy shape [Fig. 1(d)], and the SHG intensities were significantly altered [Fig. 1(e)]. In addition to intrinsic aging, changes in elastin fiber structure presumably due to photoaging (photo elastosis) was also observed [Figs. 1(f)–1(i)].

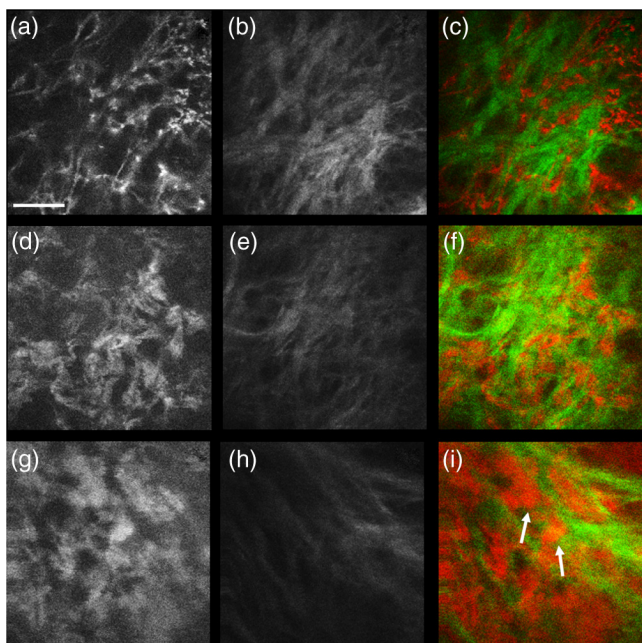*Address all correspondence to: Georgios N. Stamatas, E-mail: gstamata@its.jnj.com

Fig. 1 Representative multiphoton images of the dermis of facial skin. Younger group: (a) elastin fibers, (b) collagen fibers, and (c) false color overlay image (red: elastin fibers; green: collagen fibers); older group: (d) elastin fibers, (e) collagen fibers, and (f) false color overlay image (red: elastin fibers; green: collagen fibers); photodamaged skin (older group): (g) elastin fibers, (h) collagen fibers, and (i) false color overlay image (red: elastin fibers; green: collagen fibers). While arrows point to regions of potential photo-elastosis. Scale bar: 50 μm.

In the past, Ruvolo et al.[9] introduced the anisotropy ratio to quantify the directionality of skin surface tension. They showed that it is a sensitive parameter to capture the age-dependent preferential orientation that aligns roughly with the Langer's lines.[9] Here, we propose a similar approach, through the use of the anisotropy ratio, to evaluate the cohesiveness in the orientation of the collagen and elastin fibers on the multiphoton images. Figure 2 shows a diagram of the image analysis process we followed. Each selected ROI image was normalized to a mean intensity of zero with standard deviation of one. A 5×5 Gaussian filter with $\sigma = 1$ was used to calculate the local intensity gradient and generate the local orientation map image.[10] In
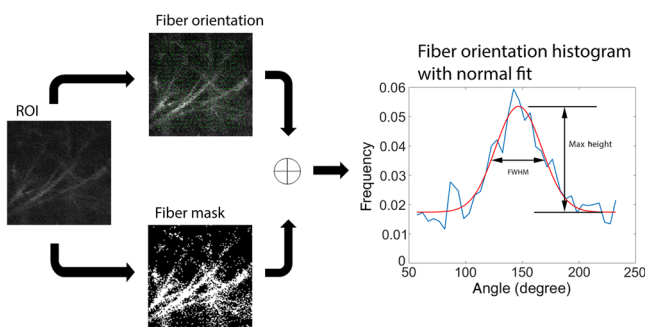

Fig. 2 Image analysis flow diagram for the calculation of the anisotropy ratio of the fiber orientation. The normalized ROI was used to generate the fiber orientation map and the fiber mask. The resulting fiber orientation histogram was approximated with a normal distribution function, which was used to calculate the anisotropy ratio of the fiber orientation.
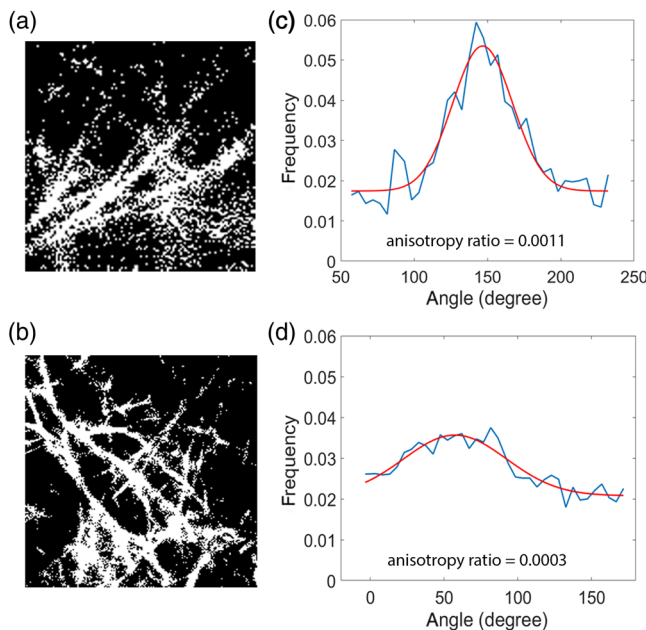

Fig. 3 Representative fiber images with (a) relatively high anisotropy ratio (0.0011) and (b) relatively low anisotropy ratio (0.0003). (c) A high anisotropy ratio value is indicative of strong fiber alignment at the dominant orientation, while (d) a low anisotropy ratio value is indicative of more random fiber orientation.

parallel, K-means clustering[11] was used to binarize the image into two clusters (fibers and background). The local fiber orientation was extracted by combining the K-means clustering and the local orientation map. Then, the orientation distribution for the fiber cluster was plotted and approximated with a normal distribution curve. From the parameters of the fitted curve, we calculated the full width at half maximum (FWHM) and the anisotropy ratio, defined as the ratio of the Gaussian maximum over the FWHM

$$\text{Anisotropy ratio} = \frac{\text{max height}}{\text{FWHM}}. \quad (1)$$

High anisotropy ratio corresponds to a strong alignment in the fiber orientation, whereas low anisotropy ratio corresponds to a more random fiber orientation (Fig. 3). Note that multiple dominant orientations may exist, which would increase the error of the normal fit. The mean square error of the fit was analyzed, and no significant difference was observed between the two age groups.

The older group showed a significantly higher anisotropy ratio compared with the younger group ($p < 0.05$), indicating that both the collagen and elastin fibers in the older group have a more aligned orientation with a strong dominant direction [Figs. 4(a)–4(b)]. Further analysis of individual sites was performed to examine the effect of photo exposure on collagen and elastin fiber orientation anisotropy. From the three sites of interest in this study, the cheek site can be considered as the most photo exposed and the upper inner arm as the least photo exposed. Collagen fibers [Fig. 4(c)] showed consistently higher anisotropy ratio for all three body sites for the older group, which suggests that increased photo exposure has minimal effect on collagen fiber orientation. The effect of photo exposure is more prominent for the elastin fibers [Fig. 4(d)]. The largest differences in the anisotropy ratio values between
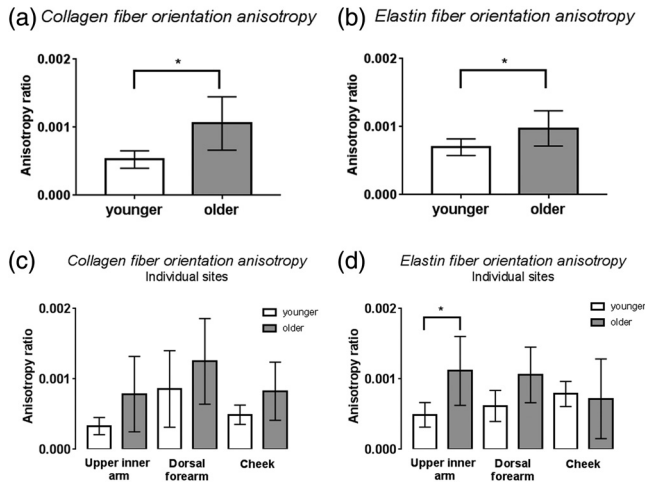
Fig. 4 Comparison of the anisotropy ratio values between the younger and the older age group for (a) collagen and (b) elastin fiber orientation. The older group shows higher anisotropy ratio values and therefore higher alignment of the fibers with a dominant orientation. Different body sites have various degrees of photo exposure. The cheek site has the highest photo exposure of the three sites tested, whereas the upper inner arm has the least photo exposure. (c) Collagen fiber orientation anisotropy is higher for the older group for the three sites measured, suggesting minimal effect of photo exposure on collagen fiber orientation. (d) Elastin fiber orientation anisotropy is significantly different between the two groups for the upper inner arm, where intrinsic aging is the primary factor. The error bar represents 95% CI and * represents significant difference ($p < 0.05$). Unpaired t-test with equal variance was used in (a) and (b) and nonparametric ANOVA with Sidak's multicomparison test was used in (c) and (d).

the two age groups were observed for the upper inner arm, where photo exposure is relatively low and intrinsic aging is the primary factor. The increased anisotropy in elastin fiber orientation may relate to reduced skin elasticity and resiliency in aged skin.[12]

Fiber density was calculated on the binarized images generated with the K-means clustering method. As shown in Figs. 5(a)–5(c), elastin fiber density is statistically higher in the older age group, independently of the body site tested. On the other hand, the collagen fiber density is lower for the older group for the cheek and dorsal forearm site but without statistical difference for the upper inner arm site. This indicates that a combination of extrinsic aging (i.e., photodamage) with intrinsic aging may synergistically elevate the degree of collagen degradation. In addition to the fiber density, the mean signal intensity of each ROI was also calculated. For facial skin, the mean signal intensity of both elastin (TPF) and collagen (SHG) fibers was found to be significantly lower in the older group compared with the younger (data not shown). However, for both the upper inner arm and dorsal forearm site, there was no statistical significance between the two age groups for either the TPF or SHG images. These results further prove that considering only the mean signal intensity is enough to differentiate between the age groups. The spatial distribution analysis provides complimentary information and can be very useful in the study of the dermal fiber remodeling processes associated with aging.

In summary, the common method of calculating SAAID based on TPF/SHG images involves the average signal intensity and neglects the spatial distribution information. In this paper, we propose a method that accounts for the spatial information,
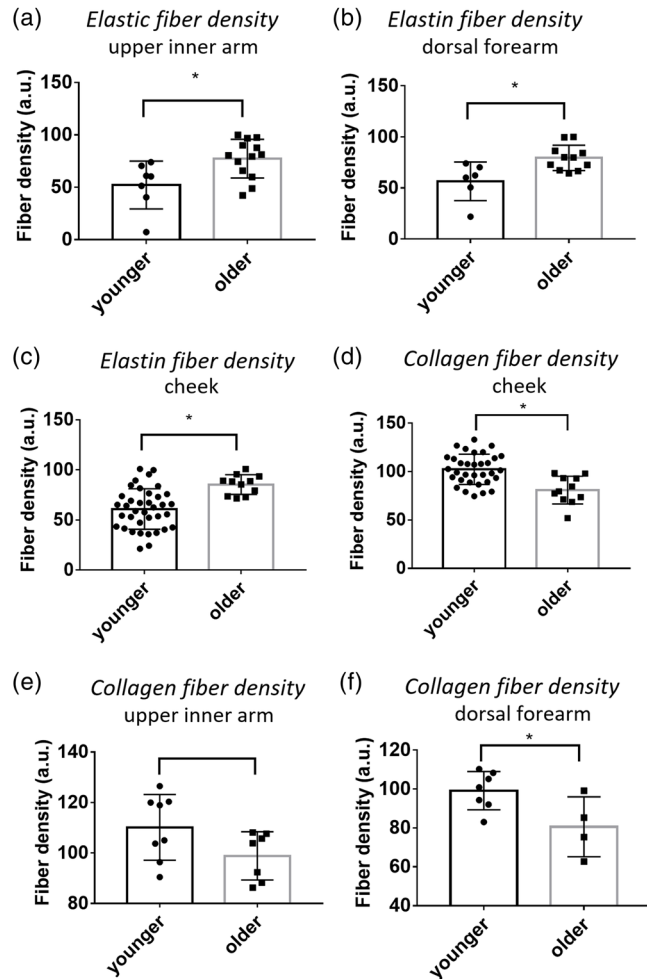

Fig. 5 Representative images and fiber density comparison between younger and older skin at different body sites. (a) Elastin fibers, upper inner arm, (b) elastin fibers, dorsal forearm, (c) elastin fibers, cheek, (d) collagen fibers, cheek, (e) collagen fibers, upper inner arm, and (f) collagen fibers, dorsal forearm. Unpaired t-test with equal variance was used, error bars represent one standard deviation, * represents significant difference ($p < 0.05$).

which provides additional insights into how collagen and elastin fibers are altered with age. Both collagen and elastin fibers showed a greater alignment of fiber orientation with one single dominant orientation in the older group. The greatest difference in elastin fiber anisotropy between the two groups was found for the upper inner arm site. Elastin fiber density increased with age, whereas collagen fiber density decreased with age.

Disclosures

All authors are employees of the Johnson & Johnson family of consumer companies.

Acknowledgments

References

1. N. Puizina-Ivic, "Skin aging," *Acta Dermatovenerol. Alp. Panonica Adriat.* **17**(2), 47–54 (2008).

2. C. Longo et al., "Skin aging: in vivo microscopic assessment of epidermal and dermal changes by means of confocal microscopy," *J. Am. Acad. Dermatol.* **68**(3), e73–e82 (2013).

3. K. Sauermann et al., "Age related changes of human skin investigated with histometric measurements by confocal laser scanning microscopy in vivo," *Skin Res. Technol.* **8**(1), 52–56 (2002).

4. S. Neerken et al., "Characterization of age-related effects in human skin: a comparative study that applies confocal laser scanning microscopy and optical coherence tomography," *J. Biomed. Opt.* **9**(2), 274–281 (2004).

5. B. Masters, P. T. So, and E. Gratton, "Multiphoton excitation fluorescence microscopy and spectroscopy of in vivo human skin," *Biophys. J.* **72**(6), 2405–2412 (1997).

6. K. König, "Clinical multiphoton tomography," *J. Biophotonics* **1**(1), 13–23 (2008).

7. M. J. Koehler et al., "Intrinsic, solar and sunbed-induced skin aging measured in vivo by multiphoton laser tomography and biophysical methods," *Skin Res. Technol.* **15**(3), 357–363 (2009).

8. S. Wu et al., "Quantitative analysis on collagen morphology in aging skin based on multiphoton microscopy," *J. Biomed. Opt.* **16**(4), 040502 (2011).

9. E. C. Ruvolo, Jr, G. N. Stamatas, and N. Kollias, "Skin viscoelasticity displays site- and age-dependent angular anisotropy," *Skin Pharmacol. Physiol.* **20**(6), 313–321 (2007).

10. A. R. Rao, *A Taxonomy for Texture Description and Identification*, Springer, New York (1990).

11. C. M. Bishop, *Pattern Recognition and Machine Learning*, Springer, New York (2006).

12. H. S. Ryu et al. "Influence of age and regional differences on skin elasticity as measured by the Cutometer®," *Skin Res. Technol.* **14**(3), 354–358 (2008).